Vietnam Journal of Science and Technology ***64***(3) (2026) 518–527
DOI: https://doi.org/10.15625/2525-2518/21444

Texture topography influence on icing repellency efficiency of nanotexture superhydrophobic surfaces

Thi Minh Thuy Nguyen, Dang Van Sang, Nguyen Thi Huong, Thanh-Binh Nguyen*

Thai Nguyen University of Education, 20 Luong Ngoc Quyen, Phan Dinh Phung ward, Thai Nguyen, Viet Nam

*Email: *binhnt@tnue.edu.vn*

Received: 16 September 2024; Accepted for publication: 6 November 2025

Abstract. In this study, we investigated the influence of surface topography on ice-phobic efficiency,including the degradation of ice-to-surface bond strength and ice resistance on superhydrophobic surfaces. Uniform nanostructures with different morphologies were generated on PDMS thin films using the spin coating technique, followed by a lift-off method combined with a hard PI (Polyimide) mold. The concept of a unit cell was proposed to investigate the contribution of nanotextures on surfaces with relatively similar wettability to bond strength. The results showed a linear dependence of the measured values on the proposed regular hexagon-shaped area fraction, confirming the importance of textured structures in ice removal performance, especially in the superhydrophobic range. In addition, the evaluation of ice resistance over time showed a great influence of the size of the surface structure on the nucleation and propagation of ice nuclei. The experimental results demonstrate the importance of the influence of surface parameters and suggest rational designs for ice-phobic surfaces.

Keywords: water repellency, surface morphology, nanostructure, hexagonal unit cell, ice resistance.

Classification numbers: 2.4, 2.5, 2.9.3.

1. INTRODUCTION

The formation of ice on surfaces near the Earth's surface often causes dangerous and unexpected risks in many cases [1–6]. Ice on aircraft wings and engines disrupts the aerodynamic structure and can cause loss of control while flying [7–9]. Thick ice accumulation on power transmission systems in cold weather often causes overloading and collapse, affecting the transmission process and posing a danger to people and infrastructure [10–14]. Ice can also easily form on ships and drilling rigs, endangering movement and work safety [4, 5, 15, 16].

Over the past few decades, research directions have focused on developing and optimizing techniques to prevent icing situations encountered in life, transportation, and industry [14, 15, 17–21]. Anti-icing methods can be defined as active or passive based on the perspective of the external energy required. While active methods focus on de-icing using heating, de-icing liquids, or vibrations to mechanically remove ice, which requires external energy [22–26], passive methods rely on surface texture modification and low surface energy to resist ice formation or delay liquid-solid phase transition without requiring any energy source [20, 27–33]

Among the passive approaches, superhydrophobic morphology is considered the most desirable solution for anti-icing applications. Recent studies have demonstrated passive anti-icing properties that reduce adhesion to the surface and maintain anti-icing surfaces under icy conditions. A standard anti-icing surface needs to include many factors such as structural calculations, surface energy, contact liquid, and specific working environment, as they determine how they react to liquids [22, 28, 34–37].

To the best of our knowledge, studies to date have focused on fine-tuning and refining the surface structure to enhance anti-icing performance in aspects including adhesion degradation, phase transition extension, or function retention under freezing conditions.

However, from a theoretical point of view, the contribution of surface morphology to ice resistance properties has not been fully investigated [37, 38], specifically compared and evaluated, especially in the very narrow range of superhydrophobicity. For example, current studies cannot explain why surfaces with similar superhydrophobic wettability have different bond strengths. In addition, the important role of structural subtlety in nucleation formation also needs to be clarified because it is related to maintaining the functionality of working surfaces under freezing conditions and thus guiding the optimization of surface properties.

In this study, we aim to investigate the influence of surface topography on ice repellency including bond strength and ice resistance on superhydrophobic surfaces in real time. Uniform nanostructures with different morphologies will be fabricated on PDMS thin films by spin coating technique followed by a lift-off method. A regular hexagonal unit cell morphology describing the surface structure is proposed to study the influence of projected area on surfaces with relatively similar wettability. The results document the important role of surface restructuring in improving ice removal performance for surfaces in the superhydrophobic range. On the other hand, the ice resistance over time demonstrates a great influence of the nanostructure size on the formation and propagation of ice nuclei. The experimental results demonstrate the importance of surface textures and suggest rational designs for ice-phobic surfaces.

2. MATERIALS AND METHODS

2.1. Materials

The investigated samples were fabricated on PDMS thin films with tailored nanotexture designs. PDMS is viscoelastic, acting as a viscous liquid at high temperatures while performing as an elastic solid at low temperatures (curing). The mechanical properties of PDMS enable it to conform to a diverse variety of surfaces owing to being easily stretched, bent, and compressed in all directions, which might be used to attach to functional surfaces working outside.

2.2. Preparation

Figure 1a describes the fabrication process (a) and the corresponding surface morphologies after the lift-off process (b-g). After the etching and lift-off routine, surfaces demonstrated the well-uniformed textures created on the PDMS thin film surface (b-g). Textured samples were then coated with FOTS (FluotoothorTetroSilane, Sigma-Aldrich Inc., USA) via vapor coating for 1 hour to enhance the hydrophobicity. After functionalization, samples demonstrated outstanding water repellency with contact angles ranging from 156°±0.3° to 159.5°±0.3° (Figure 1h).

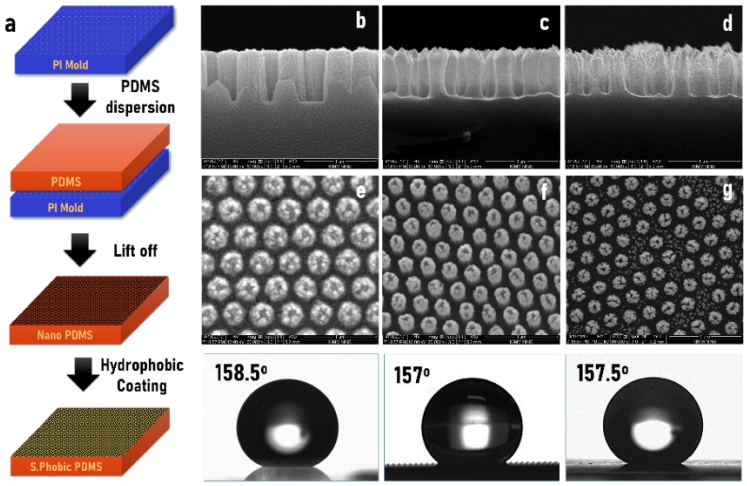

Figure 1. Fabrication process of flat and micro-groups (a), nanostructure surface with different morphologies from side view (b, c, d), top view (e, f, g), and corresponding wettability (h).

2.3. Characterization

The wettability of samples was measured using a contact angle apparatus (Kyowa Interface Science Co. Ltd., Japan) with 5-10 µL deionized water droplets [39]. The contact angle value was determined statistically by the measurement from ten independent positions on each sample (Table 1). The dynamic contact angle measurements were used to determine a deeper insight into surface properties (Figures 2a,b). By measuring the advancing and receding contact angles, we can observe the true liquid-surface interactions and intrinsic surface properties to further explain the phenomena occuring at the three-phase interface.

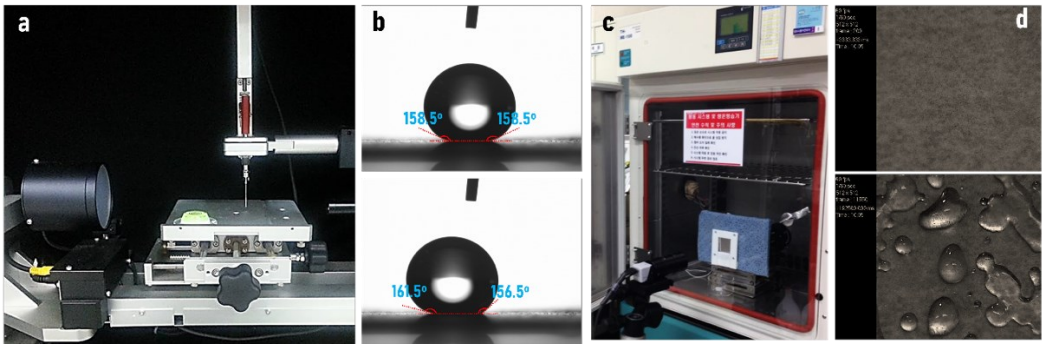

Figure 2. Dynamic contact angle measurement equipment (a), static contact angle (top), advancing and receding contact angle (bottom) (b), experimental setup for evaluating icing repellency (c), and real-time image captured from a high-speed camera (d).

Evaluated samples were carefully attached to a cooling plate using Aluminum tape set up inside the environmental chamber maintained under compared conditions in cold weather (-5 °C or 23 °F, and 75 % humidity) (Figure 2c). A high-speed camera (Photron Ltd.) was used to observe the icing process and quantitatively determine the icing resistance of each sample (Figure 2d). The anti-icing performance was observed through a computer and processed using ImageJ to determine the ice-covered area over time.

The high-speed camera was also used to determine the velocity of water droplets falling on the superhydrophobic surfaces. A stopwatch initially incorporated into high-speed camera exactly determined the position of water droplets and therefore calculated the velocity.

Table 1. Information details of all investigated samples.

No	d (nm)	s (nm)	CA (°)	SA (°)	Advancing angle (°)	Receding angle (°)	f	Adhesive strength (kPa)	Velocity (cm/s)
Bare	Bare PDMS		79±0.2	15	89±0.5	68±0.5	1	238±0.6	--
1	300	400	158.5±0.3	1.2	161.5±0.5	156.5±0.3	0.51	158.6±0.5	4.28
2	230	400	157±0.2	1	162±0.2	155.5±0.3	0.30	148.3±0.8	5.14
3	180	400	157.6±0.3	1	162.5±0.3	155±0.2	0.18	141.2±0.6	5.71

3. RESULTS AND DISCUSSION

The hydrophobicity of the fabricated surfaces was investigated using water-repellent testing, as shown in Figure 3. Dust was poured onto three superhydrophobic surfaces titled at 30°. Water droplets were gently dropped on the top edge of the sample and freely rolled down by gravity. The movement of the droplets was observed using a high-speed camera placed positioned opposite the sample surface.

Despite relatively similar hydrophobicity, the surfaces illustrate a significant difference in water-repellent efficiency. Indeed, water droplets of the same-volume present relatively different velocities. Interestingly, the water velocity shows a chaotic correlation with the contact angle. The fastest surprisingly belongs to the #3 (CA 157.6° ± 0.3) sample and gradually decreases by #2 (157° ± 0.2) and #1 (158.5° ± 0.3).

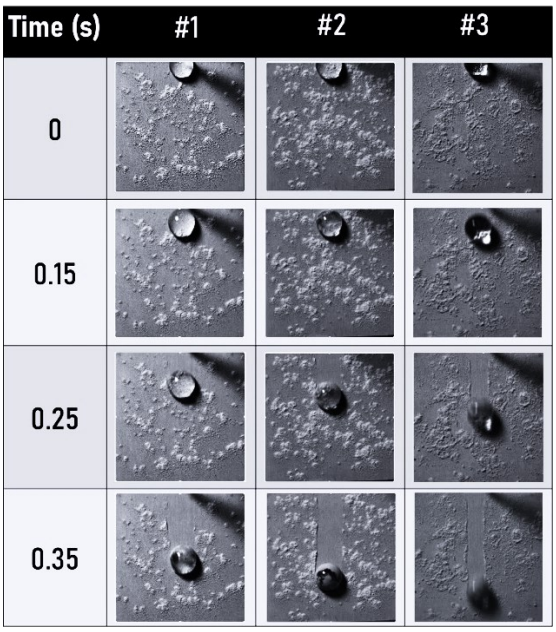

Figure 3. Water repellency and self-cleaning ability on different surfaces.

The interface contact characteristics between textures and liquid were evaluated for three nanostructure samples to consider the profound contribution of surface topography, especially

for samples with relatively similar wettability in the superhydrophobic range. Indeed, the unit cell index was brought into consideration, demonstrating the importance of texture properties in adhesion reduction. Figure 4 describes our proposed unit cell definition with an area fraction *f* in a hexagon shape with s and d parameters, corresponding to the center-to-center spacing and pillar diameter, respectively. It should be noted here that the *f* strongly depends on the surface parameters such as diameter, and spacing, which is believed to determine the Laplace pressure acting at the curvature given by neighbor nanopillars. The higher area fraction refers to the larger contact area between surface textures and water droplets. With a given spacing s, the lowering of diameter d leads to the longer air-water interface, leading to the higher Laplace pressure acting at the air-water curvature and significantly affecting the three-phase boundary's contact angle. However, the qualitative contact angle might not be solely used to determine the surface characteristics including adhesion strength or water repellency.

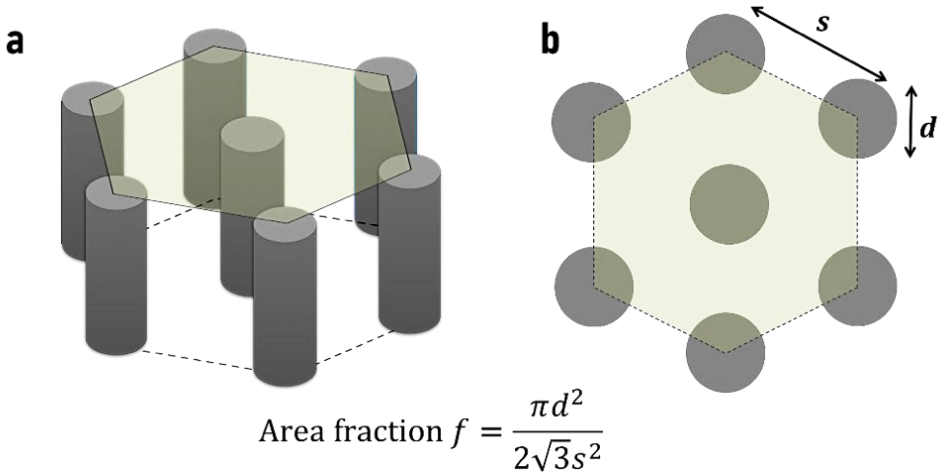

Figure 4. Proposed model of area fraction *f* from tilted view (a) and top view (b).

Figure 5 illustrates the fit of the ice-surface adhesion (left) and contact angle (right) plotted against the area fraction and shows the different distributions on each criterion. It is important to note that the results were measured at least 10 times on the same sample to determine the average value. The blue bars represent the values measured on samples #1, #2, and #3 in comparison to the bare sample. The dashed lines represent the wettability of the superhydrophobic samples with small differences between the measured contact angles. Interestingly, larger contact angles might not ensure smaller bond strength. Indeed, sample #1 has the largest contact angle and surprisingly decreases as the nanopillars become sharper.

On the other hand, the area fraction *f* illustrates an inverse correlation with the measured adhesion strength and is considered a reliable indicator for optimizing the anti-icing performance. Figure 5 (blue column) reveals good agreement with the area fraction *f* indicated in Table 1. The mechanism might be attributed to the projected contact area at the interface [37]. In the relatively similar wetting state, the lower area fraction corresponds to the narrower contact area. Indeed, the lowest value belongs to #3 (0.18) and gradually increases with the increase of *f*.

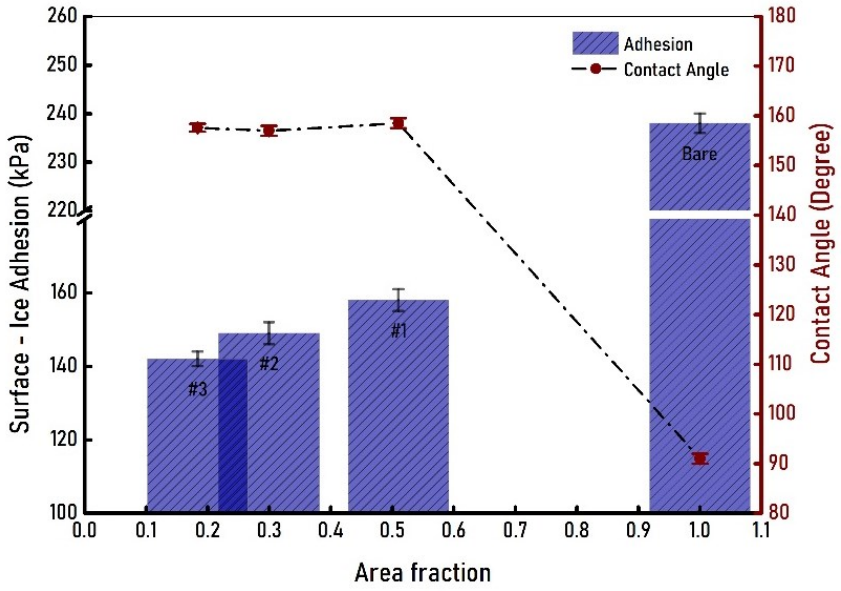

Figure 5. Adhesion strength and contact angle plotted against area fraction.

Recent studies across a wide range, from superhydrophilic to superhydrophobic, may readily explain the aforementioned relationship owing to the large difference between contact angle and contact area [29, 40, 41]. The larger the contact angle, the smaller the area fraction, meaning there is less contact area between the ice and the surface structure. Bond strength is essentially an electrostatic interaction between charges at the interface and therefore depends on the interface's nature and contact area. Meanwhile, the contact angle in the very narrow superhydrophobic range may not facilitate a good indication as it cannot show any familiar trends or relationships with the measured adhesion values. This can be explained by the penetration of water between the nanostructures, which may affect the contact behavior. As the tips of the pillars become smaller, the distance between them becomes larger, thus facilitating water penetration. During this propagation, the Laplace pressure directed from the inside exerts a larger pressure on the curved interface and thus slightly shrinks the contours at the three-phase interface, resulting in a slight decrease in the contact angle from sample #1 to sample #3. Furthermore, the longer air-water curvature enhances the sagging effect before freezing, therefore facilitating the anchoring effect at the pillars' edge, which significantly increases the adhesion. Hence, the area fraction f will quantitatively determine the surface-ice adhesion strength and should be documented as an icephobic effectiveness index.

Until now, the inverse correlation between anti-icing and wettability has been demonstrated for several decades [20, 32, 42]. However, in this work, the relative samples' contact angle reveals an appreciable difference in ice resistance over time and documents an interesting phenomenon. Figure 6 reveals the icing evolution on superhydrophobic surfaces with relative differences in icing resistance. Interestingly, the anti-icing performance may not be effectively used to explain this behavior based on previous research, and this raises a remarkable question.

As shown in Figure 6, the sample #3 can maintain a clear area (black) that is much larger than other surfaces after 60 minutes. The ImageJ software has been used to qualitatively measure the ice-covered area (white) on different surfaces. After one hour, the ice covers over

80 % and 75 % of samples #1 and #2, respectively. On the opposite side, the clean area still maintains around 50 % on the #3 surface, corresponding to increases of 183 % and 104 % compared to the samples #1 and #2, respectively. It can be explained by the area fraction criterion and surface textures while the spacing plays an important role in determining the nuclei radius. The higher area fraction corresponds to the larger contact area between the surface textures and water within the same cross-section of the unit cell. From the perspective of heat conduction coefficient, the heat is mainly transmitted through the PDMS-water area. Therefore, the lower the area fraction we can generate, the lower the heat transferred through the interface per unit time.

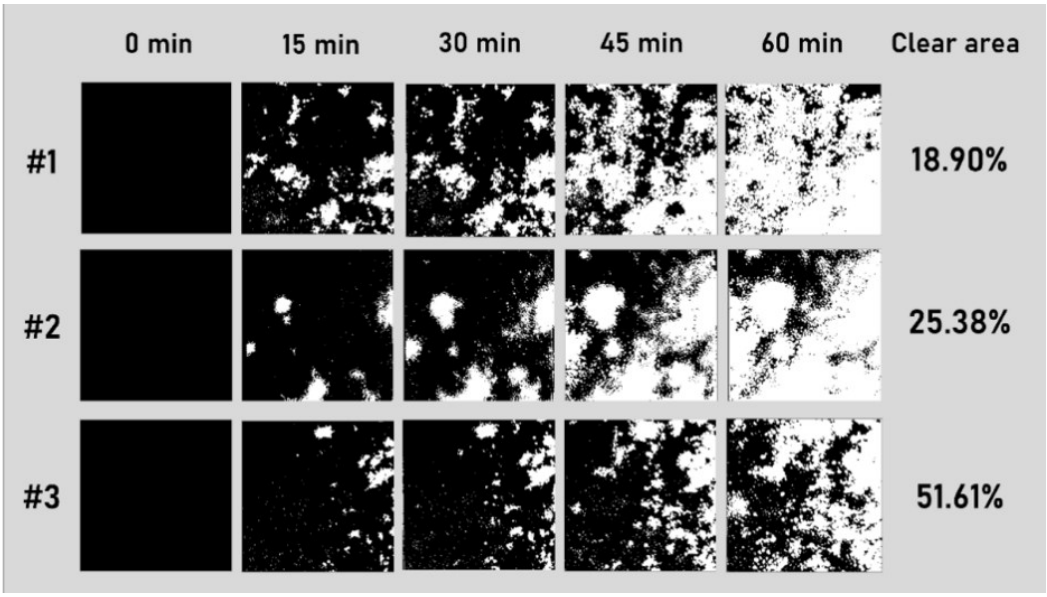

Figure 6. Icing evolution on different morphologies and ice resistance performance with corresponding clear areas.

4. CONCLUSIONS

In this work, we comprehensively evaluated the effects of surface topography on anti-icing performance in terms of ice repellency and ice-surface adhesion deterioration. The unit cell structure was introduced to clarify the differences in bonding strength and ice resistance of surfaces in the superhydrophobic range. The area fraction was evaluated, demonstrating a crucial role in the prediction of the adhesion strength on uniform nanostructure. An icing test was proposed to examine the contribution of surface textures to determining ice formation on functional surfaces. This advantage can be explained by the unique morphology to enhance water repellency and therefore inhibit ice nucleation and coalescing behavior of neighbor droplets. Our research results document the importance of the design for functional surfaces in both adhesion strength and ice resistance for potential outdoor applications.

Acknowledgements. The research is funded by the Vietnam National Foundation for Science and Technology Development (NAFOSTED) under grant number 103.02-2023.106

CRediT authorship contribution statement. Thi Minh Thuy Nguyen: Investigation, Writing-original draft; Dang Van Sang, Nguyen Thi Huong: Investigation, Data Curation; Thanh-Binh Nguyen:

Conceptualization, Methodology, Supervision, Writing-review&Editing. All authors have read and agreed to the published version of the manuscript

Declaration of competing interest. The authors declare no competing interests.

REFERENCES

1. Wang G., Xu H., Pei B. – An intelligent approach for flight risk prediction under icing conditions. Chin. J. Aeronaut., **36** (2023) 109–127. https://doi.org/10.1016/j.cja.2023.02.020.
2. Hann R., Enache A., Nielsen M. C., et al. – Experimental heat loads for electrothermal anti-icing and de-icing on UAVs. Aerospace, **8** (2021) 83. https://doi.org/10.3390/aerospace8030083.
3. Liu Q., Yang Y., Wang Q., Cui Y., Cai J. – Icing performance of stratospheric airship in ascending process. Adv. Space Res., **64** (2019) 2405–2416. https://doi.org/10.1016/j.asr.2019.09.013.
4. Samuelsen E. M. – Ship-icing prediction methods applied in operational weather forecasting. Q. J. R. Meteorol. Soc., **144** (2018) 13–33. https://doi.org/10.1002/qj.3174.
5. Samuelsen E. M., Graversen R. G. – Weather situation during observed ship-icing events off the coast of Northern Norway and the Svalbard archipelago. Wea. Climate Extremes, **24** (2019) 100200. https://doi.org/10.1016/j.wace.2019.100200.
6. Cheng X., Shi F., Liu Y., Liu X., Huang L. – Wind turbine blade icing detection: A federated learning approach. Energy, **254** (2022) 124441. https://doi.org/10.1016/j.energy.2022.124441.
7. Olejniczak D., Nowacki M. – Evaluation of the influence of icing on wings on aircraft flight parameters. Transp. Res. Procedia, **35** (2018) 100–109. https://doi.org/10.1016/j.trpro.2018.12.017.
8. Wisdom K. M., Watson J. A., Qu X., Liu F., Watson G. S., Chen C.-H. – Self-cleaning of superhydrophobic surfaces by self-propelled jumping condensate. Proc. Natl. Acad. Sci. U.S.A., **110** (2013) 7992–7997. https://doi.org/10.1073/pnas.1210770110.
9. Yamazaki M., Jemcov A., Sakaue H. – A review on the current status of icing physics and mitigation in aviation. Aerospace, **8** (2021) 188. https://doi.org/10.3390/aerospace8070188.
10. Farzaneh M., Volat C., Leblond A. – Anti-icing and de-icing techniques for overhead lines. In: Farzaneh M., ed. *Atmospheric icing of power networks*. Springer Netherlands, Dordrecht, (2008) 229–268. https://doi.org/10.1007/978-1-4020-8531-4_6.
11. Laforte J. L., Allaire M. A., Laflamme J. – State-of-the-art on power line de-icing. Atmos. Res., **46** (1998) 143–158. https://doi.org/10.1016/s0169-8095(97)00057-4.
12. Zarnani A., Musilek P., Shi X., Ke X., He H., Greiner R. – Learning to predict ice accretion on electric power lines. Eng. Appl. Artif. Intell., **25** (2012) 609–617. https://doi.org/10.1016/j.engappai.2011.11.004.
13. Zhao Q., Liu Z., Yu P., Chen L., Guan F. – Review of transmission line icing and anti-icing technologies. In: Liang X., Li Y., He J., Yang Q., eds. *The proceedings of the 16th annual conference of china electrotechnical society*. Springer Nature Singapore, Singapore, (2022) 1224–1232. https://doi.org/10.1007/978-981-19-1870-4_129.
14. Wen S. F., Wang Y. M., Zhang Z. M., Liu Y. L. – Application of anti-icing coating based on adsorption of functional substances by microporous sphere. Prog. Org. Coat., **137** (2019) 105320. https://doi.org/10.1016/j.porgcoat.2019.105320.
15. Zhang Y., Zhang L., Luo G. – Study on de-icing criterion of anti-icing coating and simulation analysis method of mechanical de-icing process for polar ship superstructure. Ocean Eng., **288** (2023) 115811. https://doi.org/10.1016/j.oceaneng.2023.115811.
16. Liu Y., Li X., Jin J., et al. – Anti-icing property of bio-inspired micro-structure superhydrophobic surfaces and heat transfer model. Appl. Surf. Sci., **400** (2017) 498–505. https://doi.org/10.1016/j.apsusc.2016.12.219.
17. He J., Wang J., Wang R., et al. – Preparation and anti-icing performance of liquid lubricant micro-nano composite coating based on modified nano-SiO_2. J. Adhes. Sci. Technol., **37** (2023) 2139–2153. https://doi.org/10.1080/01694243.2022.2117643.

18. Meng Y., Zhang C., Chen J., et al. – Deicing characteristics and pavement performance of eco-friendly de-icing asphalt mixture. Constr. Build. Mater., **360** (2022) 129565. https://doi.org/10.1016/j.conbuildmat.2022.129565.
19. Hanh V. T. H., Truong M. X., Nguyen T.-B. – Anti-icing approach on flexible slippery microstructure thin-film. Cold Regions Sci. Technol., **186** (2021) 103280. https://doi.org/10.1016/j.coldregions.2021.103280.
20. Zhang S., Gao F., Jiang Z., et al. – Bioinspired durable interpenetrating network anti-icing coatings enabled by binders and hydrophobic-ion specific synergies. Chem. Eng. J., **479** (2024) 147836. https://doi.org/10.1016/j.cej.2023.147836.
21. Hanh V. T. H., Chi D. T., Ha C. V., et al. – Icephobic approach on hierarchical structure polymer thin-film. Adv. Nat. Sci: Nanosci. Nanotechnol., **13** (2022) 015004. https://doi.org/10.1088/2043-6262/ac5400.
22. Zehui Z., Zelinlan W., Guang L., et al. – Liquid-like slippery surface with passive-multi active strategy integration for anti-icing/de-icing. Chem. Eng. J., **474** (2023) 145541. https://doi.org/10.1016/j.cej.2023.145541.
23. Chen J., Yuan X., Liu Q., Zhang W., Huang J. – Mechanical, anti-icing and de-icing performance of porous asphalt mixture containing chloride-based particle. Int. J. Pavement Eng., **24** (2023) 2262087. https://doi.org/10.1080/10298436.2023.2262087.
24. Jia Y., He Q., Liu Y., Xu Y., Wang J., Li A. – Anti-icing system based on multi-level micro-nano and electric heating dual structure. Colloids Surf. A, **683** (2024) 133105. https://doi.org/10.1016/j.colsurfa.2023.133105.
25. Liu Y., Sun H., Song X., Liu C. – A mechanically durable induction heating coating with desirable anti-/de-icing performance. Surf. Eng., **39** (2023) 413–420. https://doi.org/10.1080/02670844.2023.2229563.
26. Mu Z., Guo W., Li Y., Tagawa K. – Wind tunnel test of ice accretion on blade airfoil for wind turbine under offshore atmospheric condition. Renewable Energy, **209** (2023) 42–52. https://doi.org/10.1016/j.renene.2023.03.126.
27. Rui Y., Yu B., Liu Y., Fu L., Liu J., Lu G. – Hydrophilic coating with anti-fogging and anti-icing properties. J. Macromol. Sci. Part B, **63** (2024) 47–59. https://doi.org/10.1080/00222348.2023.2251309.
28. Wu L., Liu P., Hua X., Guo Z., Liu W. – Photothermal superhydrophobic membrane based on breath figure: Anti-icing and deicing. Chem. Eng. J., **480** (2024) 147553. https://doi.org/10.1016/j.cej.2023.147553.
29. Cui Y., Zhang L., Xing C., Tan Y. – Anti-icing properties and application of superhydrophobic coatings on asphalt pavement. Constr. Build. Mater., **419** (2024) 135452. https://doi.org/10.1016/j.conbuildmat.2024.135452.
30. Kuai S., Tang J., Zhou L., et al. – Durable anti-icing coating with stability based on self-regulating oil storage layer. Colloids Surf. A, **685** (2024) 133028. https://doi.org/10.1016/j.colsurfa.2023.133028.
31. Zhou L., Liu A., Tang J., et al. – Mechanically robust liquid-embedded coating with anti-icing/deicing durability. Colloids Surf. A, **674** (2023) 131924. https://doi.org/10.1016/j.colsurfa.2023.131924.
32. Zeng D., Li Y., Liu H., et al. – Superhydrophobic coating induced anti-icing and deicing characteristics of an airfoil. Colloids Surf. A, **660** (2023) 130824. https://doi.org/10.1016/j.colsurfa.2022.130824.
33. Nguyen T.-B., Boudkhamchampa K., Bui T. T., Dang M. H. – Facile approach for omniphobic and anti-icing on Fe surface. Commun. Phys., **33** (2023) 85. https://doi.org/10.15625/0868-3166/17451.
34. Heymsfield E., Daniels J. W., Saunders R. F., Kuss M. L. – Developing anti-icing airfield runways using surface embedded heat wires and renewable energy. Sustainable Cities Soc., **52** (2020) 101712. https://doi.org/10.1016/j.scs.2019.101712.
35. Mrsic I., Bäuerle T., Ulitzsch S., et al. – Oxygen plasma surface treatment of polymer films-Pellethane 55DE and EPR-g-VTMS. Appl. Surf. Sci., **536** (2021) 147782. https://doi.org/10.1016/j.apsusc.2020.147782.

36. Xu Z., Zhang T., Li X., Li Y. – Effects of ambient temperature and wind speed on icing characteristics and anti-icing energy demand of a blade airfoil for wind turbine. Renewable Energy, **217** (2023) 119135. https://doi.org/10.1016/j.renene.2023.119135.
37. Truong M. X., Hanh V. T. H., Nguyen T.-B. – The integrated contribution of surface topology to anti-icing effectiveness. Surf. Topogr. Metrol. Prop., **10** (2022) 015036. https://doi.org/10.1088/2051-672x/ac56a8.
38. Zhou L., He W., Wang M., Hou X. – Enhanced phase-change heat transfer by surface wettability control. ChemSusChem, **15** (2022) e202102531. https://doi.org/10.1002/cssc.202102531.
39. Nguyen V.-H., Nguyen B. D., Pham H. T., et al. – Anti-icing performance on aluminum surfaces and proposed model for freezing time calculation. Sci. Rep., **11** (2021) 156. https://doi.org/10.1038/s41598-020-80886-x.
40. Ge Q., Raza A., Li H., Sett S., Miljkovic N., Zhang T. – Condensation of satellite droplets on lubricant-cloaked droplets. ACS Appl. Mater. Interfaces, **12** (2020) 22246–22255. https://doi.org/10.1021/acsami.9b22417.
41. Raiyan A., Mohammadian B., Sojoudi H. – Droplet dynamics and freezing delay on nanoporous microstructured surfaces at condensing environment. Coatings, **11** (2021) 617. https://doi.org/10.3390/coatings11060617.
42. Chen Q., Fang M., Guo R., et al. – Multi-functional and durable anti-corrosion coatings with hydrophobic, freeze time retardation and photothermal properties by means of a simple spraying method. Colloids Surf. A, **679** (2023) 132549. https://doi.org/10.1016/j.colsurfa.2023.132549.